Astronomy & Astrophysics manuscript no. output
January 19, 2023

Specialization Project

How do supermassive black holes co-evolve with their host galaxy – the perspective of cosmological simulations

P. Boccard[1], M. Hirschmann[1], F Courbin[1], J. Blunier[1]

[1]Ecole Polytechnique Fédérale de Lausanne (EPFL), Switzerland

January 19, 2023

ABSTRACT

Throughout this report, we study three black hole mass - host galaxy correlations, using the cosmological simulations of the IllustrisTNG project. In particular, we study three scaling relations : the black hole - stellar mass $M_\bullet - M_*$, the black hole - velocity dispersion $M_\bullet - \sigma$ and black hole - dark matter halo mass $M_\bullet - M_{DM}$. We conduct these studies starting at redshift $z = 0$ and then focusing on their redshift evolution and the impact of the type of galaxies and type of TNG simulations considered. Our analysis indicate that TNG100 is able to retrieve a correlation in good agreement with observations at $z = 0$ for the $M_\bullet - M_*$ relation. However the simulation produces a tighter relation than the observations and has difficulties recreating galaxies with both high-mass black hole and stellar mass typically present in observational datasets. TNG100 also produces correlations for $M_\bullet - \sigma$ and $M_\bullet - M_{DM}$ but the discrepancies with the observed relations are more pronounced. The simulated $M_\bullet - \sigma$ relation is not steep enough and is also off-setted with respect to σ, with σ being too low compared to observations. The $M_\bullet - M_{DM}$ correlation is in good agreement for $M_* < 10^{12}$ with a slope of ~ 2.7 and ~ 2.6 for observations and simulations respectively. Galaxies with $M_* > 10^{12}$ however present a discrepancy in the slopes, with a slope of ~ 0.34 and ~ 0.76 for observations and simulations respectively. Our findings also show that for the time evolution of the $M_\bullet - M_*$ relation, galaxies with a stellar mass smaller than $\sim 10^{9.5} M_\odot$ at redshift $z \sim 7$ present two phases of BH growth. During the first phase they practically don't grow while the stellar mass rapidly increases, then they grow efficiently and galaxies faithfully follow the observed relation on the $M_\bullet - M_*$ diagram. We also found that the final stellar mass of a galaxy is not correlated to its initial stellar mass as galaxies with a similar initial stellar mass can end up having a broad range of final stellar mass. Finally, for the $M_\bullet - M_*$ correlation, all simulations and type of galaxies considered give similar results in agreement with observations, with TNG100 giving the best result. As for the $M_\bullet - \sigma$ relation, it seems that no simulation is able to produce results in agreement with the observations, although TNG300 results are the closest to observations. As for the $M_\bullet - M_{DM}$ relation, we see how the simulations struggle to produce results in agreement with observations when galaxies are splitted into two dark matter mass bins. However all simulations are in good agreement with observations when the galaxies are considered all together.

1. Introduction

In the center of most galaxies lies a black hole of tremendous size and of mass of million or billions times the mass of the Sun. These are called supermassive black holes (SMBH) and it is very likely that they existed since the early ages of the Univserse, as suggested by recent observations of these objects at high redshift (Bañados et al. (2018) Mortlock et al. (2011)). Several recent studies have constructed a list of galaxies and their properties throught dynamic measurements (Kormendy & Ho (2013), Saglia et al. (2016), van den Bosch (2016)) which allow scientists to realize more direct and statistical studies of how black holes and galactic properties correlate with one another. The main focus of this study is to explore possible relations between their evolution and their host galaxy's evolution.

The first possible evidence supporting the idea of co-evolving galaxies and SMBHs is the radiation feedback induced by the black hole to the center of the galaxy. When SMBHs accrete mass at the center of the galaxy, they are known as active galactic nuclei (AGN). They induce emission of radiation, winds and jets of matter into the host galaxy, a process called AGN feedback. This phenomenon can be observed in a broad range of redshifts and various studies in the literature have reported such phenomenon (see review by McNamara & Nulsen (2007), Fabian (2012), Kormendy & Ho (2013), Kauffmann & Haehnelt (2000), Croton et al. (2006), Cattaneo et al. (2009), Fabian (2012), Cicone et al. (2014)).

If the accretion rate of the black hole is high, the center of the galaxy is then called a quasar and the radiant energy is so great that it can outshine the luminosity of the host galaxy. This feedback can be observationally measured using broad absorption line (Leighly et al. (2014)), winds seen close to the nuclei (Chartas et al. (2003), Moe et al. (2009), Tombesi (2015)) and outflows on kpc or even larger galacticscales (Cano-Díaz et al. (2012), Arav et al. (2013), Carniani et al. (2015), Choi et al. (2018), Feruglio et al. (2015)).

The second possible evidence that encourages a co-evolving galaxies and SMBHs hypothesis is the existence of a number of scaling relations between the mass of the SMBHs and different properties of the host galaxy. Among these properties are multiple photometric properties that have been identified : the total luminosity (Kormendy & Gebhardt (2001), Kormendy et al. (2011)), the bulge near-infrared luminosity (Marconi & Hunt (2003), McLure & Dunlop (2002), Graham (2007), Hu (2009)), the bulge optical luminosity (Kormendy & Richstone (1995), Kormendy & Gebhardt (2001), Schulze & Gebhardt (2011)), the blue luminosity L_B of the host bulge (Kormendy

& Richstone (1995)) and theluminosity and mass of the bulge (Kormendy (1993), Gültekin et al. (2009b)).

On top of that, the most compelling correlations concern the SMBH mass and the stellar velocity dispersion of the bulge (e.g., Ferrarese & Merritt (2000), Gebhardt et al. (2000), Merritt & Ferrarese (2001), Tremaine et al. (2002),Wyithe (2006), Hu (2008), Gültekin et al. (2009b), Schulze & Gebhardt (2011), McConnell et al. (2011a), Graham et al. (2011), Beifiori et al. (2012), Gebhardt et al. (2000), Greene et al. (2010), McConnell & Ma (2013), Kormendy & Ho (2013)). Other tight correlations with the SMBHs mass are the stellar mass of the bulge (McConnell & Ma (2013), Marconi & Hunt (2003), Häring & Rix (2004), Gadotti & Kauffmann (2009), Sani et al. (2011)), the dynamical mass of the dark matter halo (Ferrarese (2002), Baes et al. (2003), Schulze & Gebhardt (2011), Sabra et al. (2015)). finally there also exists a correlation between the SMBH mass and the total stellar mass of the galaxy (Reines & Volonteri (2015), Terrazas et al. (2016), Shankar et al. (2019)). Nonetheless, the co-evolution of the black hole and its host galaxy is a subject of debate (Kormendy & Ho (2013)). There are also studies such as (Anglés-Alcázar et al. (2013)) that have reported a possible black hole - galaxy correlation using simulations without AGN feedback or self-regulation.

We propose to study the scaling relations and their evolution with redshift using existing hydrodynamical cosmological simulations and to compare the results to existing observational data from the literature detailed in Section 3. For that we will use the simulations from the IllustrisTNG project (Nelson et al. (2018), Marinacci et al. (2018), Pillepich et al. (2018), Naiman et al. (2018), Springel et al. (2018)) and (Nelson et al. (2019), Pillepich et al. (2019)) which offer three different sizes of box for the simulations : 50, 100 and 300Mpc as we explain in more details in Section 2. On top of verifying if simulated models can replicate real phenomenons and objects in the Universe, the TNG project could allow to gain more insight into how SMBHs accrete matter or how their radiative feedback influences the properties of the host galaxy.

We motivate the use of hydrodyynamical cosmological simulations as recent progress have allowed to numerically reproduce galaxy formation and evolution by implemanting in various ways numbers of physical processes. Notably, apart from the Illustris and IllustrisTNG simulations, multiple simulations have been developped, such as Horizon-AGN (Volonteri et al. (2016)), EAGLE (Schaye et al. (2015), McAlpine et al. (2016), Rosas-Guevara et al. (2016)) and SIMBA (Davé et al. (2019), Thomas et al. (2019)). Cosmoligical simulations are now able to reproduce for example AGN feedback, galactic winds, black hole accretion, star formation or stellar mass content. On a cosmological scale, these simulations are also able to reasonably reproduce phenomenons such as galaxy clustering, merging and haloes formation (Omma et al. (2004), Choi et al. (2012), Booth & Schaye (2009), Springel et al. (2005), Faucher-Giguère & Quataert (2012), Debuhr et al. (2011), Ciotti & Ostriker (2001), Koudmani et al. (2021)). Thus, such advanced and complex hydrodynamical simulations are nowadays also able to retrieve with reasonable agreement some galaxy correlations such as the black hole and stellar mass function (Schaye et al. (2015), Nelson et al. (2018), J.Blunier report) and more importantly for us, some BH - host galaxy scaling relations observed (Li et al. (2020), Sijacki et al. (2015), McAlpine et al. (2017) and Weinberger et al. (2018)). However, these simulations still need improvements to reproduce completely and faithfully the Univserse we observe; future generations of cosmological simulations could eventually achieve this feat if the limitations of today's simulations are understood and corrected. Therefore, confronting correlations obtained with IllustrisTNG to the observed ones could be a remarkable to point out the aspects that need improvement, provided that it is understood how each numerical implementation affects the simulation.

We structure this paper as follows : Section 2 presents the key aspects of the IllustrisTNG simulations, Section 3 describes the observational data we took from the literature to compare to our simulations. We will then examine in Section 4 how we computed and simulated the galaxies properties we use and finally present some different scaling relations between the SMBH mass and the host galaxy in Section 5, comparing them with some observed ones. These scaling relations will in a first time be studied at redshift $z = 0$ and then we will examine how they evolve with time (i.e. with redshift), how they change depending on different TNG simulations or different type of galaxies considered. We present our conclusions and possible propositions for improvement in Section 6.

2. IllustrisTNG simulation

The IllustrisTNG project, the successor to the original Illustris simulation, is an ongoing series of large-scale cosmological magnetohydrodynamical simulations that take into account several physical processes. It aims to understand when and how galaxies evolve into the structures that are observed in the night sky, and to make predictions for current and future observational programs. The simulations use a state of the art numerical code using the moving mesh code AREPO. As mentionned, the project includes three primary runs spanning a range of volume and resolution, these are called TNG50, TNG100, and TNG300.

TNG300 has a periodic box $L = 205h^{-1}$ Mpc which is $\sim$ 300 Mpc on a side and a particle/cell number of 22500^3. The simulation series TNG100 has a box of intermediate size, $L = 75h^{-1}$Mpc $\sim$ 100 Mpc and uses a particle/cell number of 21820^3 at its highest resolution, the same as the Illustris simulation. Finally, TNG50 has a small box with $L = 35h^{-1}$ Mpc $\sim$ 50 Mpc and up to 22160^3 resolution elements.

The difference in size of the boxes allows them to compliment each other as TNG50 allows to reach a higher mass resolution ($\sim$ 100 times higher than TNG300) while being limited in the sampling of rare objects. The TNG50 simulation is therefore better to study structures such as individual galaxies, structures of gas around a galaxy, star formation areas in a galaxy and galactic outflows driven by supernovae and black hole feedback. On the other hand, the largest one, TNG300 enables to study galaxy clustering, to analyse rare objects such as galaxy clusters and to provide the largest galaxy sample.

Finally, TNG100 is the successor to the original Illustris simulation as it uses the same initial conditions as used in the Illustris simulation, which facilities clean comparisons between the original Illustris results and the updated TNG mode. TNG100 presents some advantages and inconveniences of the other two simulations and in this work, we will mainly work with the TNG100 simulation as it is a good compromise of both TNG300 and TNG50. However we will still compare the results with the other two simulations in order to understand the limits of each model.

The IllustrisTNG simulations use cosmological parameters taken from the Planck intermediate results : $\Omega_M = 0.3089$, $\Omega_\Lambda = 0.6911$, $\Omega_b = 0.0486$, $h = 0.6774$ and $\sigma_8 = 0.8159$. The simulations are evolved to the present epoch from $z = 127$ initial conditions. On top of this numerical framework, the TNG galaxy formation model includes some key physical processes needed to study the formation and evolution of galaxies : star formation in the dense interstellar medium, stellar feedback driven galactic-scale outflows , formation, merging, and accretion of nearby gas by supermassive blackholes, multi-mode blackhole feedback operating in a thermal 'quasar' mode at high accretion states, and a kinetic 'wind' mode at low accretion states.

In particular, modelling AGNs in cosmological simulations poses several fundamental challenges and the authors of the project had to implement for example a black hole seeding, a black hole accretion rate and black hole feedback model. For deciding the accretion state of the black hole, they use the Eddington ratio. Specifically they assume SMBHs to be in the high accretion state as long as their Bondi-Hoyle-Lyttleton accretion rate $\dot{M}_{Bondi}$ exceeds a fraction χ of the Eddington accretion rate $\dot{M}_{Edd} : \chi = \dot{M}_{Bondi}/\dot{M}_{Edd}$, with

$$\dot{M}_{Bondi} = \frac{4\pi G^2 M_{BH}^2 \rho}{c_s^3} \ , \ \dot{M}_{Edd} = \frac{4\pi G M_p}{\epsilon_r \sigma_T c} \tag{1}$$

Here, G denotes the gravitational constant, c the vacuum speed of light, m_p the proton mass and σ_T the Thompson cross-section. The factor ϵ_r is the radiative accretion efficiency, ρ and c_s are the density and sound speed of the gas near the black hole, respectively. For the black hole seeding model, the TNG simulations places a mass $M_{\rm seed}$ at the center of a galaxy (i.e. a halo) whenever the halo finder identifies a halo more massive than a threshold mass that does not yet contain a black hole. The authors adopted a black hole seed mass of $8 \cdot 10^5 \mathrm{h}^{-1} M_\odot$ which is $1.18 \cdot 10^6 M_\odot$ for haloes above $7.38 \cdot 10^{10} M_\odot$. finally, they explain that two-body discreteness effects and numerical N-body noise can displace black hole particles from halo centers. To prevent this phenomenon from happening, they force the black hole to be very close to the potential minimum of their host dark matter haloes.

finally, we point out that in the TNG simulations, it is possible to consider all galaxies in a snapshot or only select galaxies that are in the center of a halo of galaxies, we call these central galaxies. We will work on the differences TNG produces when considering central galaxies or all galaxies.

3. Observational data

For the last few decades, numerous observation programs have allowed to construct an important dataset of key galaxy properties measurements. We now have access to numerous measurements of SMBHs mass, bulge stellar mass and stellar velocity dispersion, as well as circular velocity. In our studies, all the galaxies taken from the literature are considered to be at redshift $z \sim 0$, as all galaxies are at distance $D < 300$Mpc. Measuring properties such as the stellar mass and the velocity dispersion for galaxies much more far from us reveals to be too chalenging and prone to mistakes. Here are he principal studies from which we use an observable dataset.

3.1. Datasets from McConnell & Ma (2013)

The observational data from this study will enable us to compare it to our simulations for both $M_\bullet - \sigma$ and $M_\bullet$- stellar mass relations. The authors use a sample of 72 black holes and their host galaxies updated from one of their previous study (McConnell et al. (2011b)) to which they added materials from McConnell et al. (2012), Jardel et al. (2011) and Walsh et al. (2012).

Velocity dispersion

We first use the velocity dispersion σ for which the authors present two different definitions. Both of them use spatially resolved measurements of the line-of-sight velocity dispersion σ(r) and radial velocity $v(r)$, integrated out to one effective radius (r_{eff}):

$$\sigma^2 \equiv \frac{\int_{r_{min}}^{r_{eff}} [\sigma^2(r) + v^2(r)] I(r) dr}{\int_{r_{min}}^{r_{eff}} I(r) dr} \tag{2}$$

with $I(r)$ being the galaxy's one-dimensional stellar surface brightness profile. The fist definition of velocity dispersion, that we call σ_1, takes as a lower integration limit $r_{min} = 0$ which therefore includes signal from within the black hole radius of influence, $r_{inf} = \mathrm{GM}\sigma 2$. The authors precise that in the most massive elliptical galaxies in particular, σ_1 decreases substantially when spatially resolved data within r_{inf} are excluded. They explain that the second definition, that we call σ_2, takes $r_{min} = r_{inf}$ and reflects the global structure of the galaxy and is less sensitive to angular resolution. Therefore we will take into account σ_2 to compare the observational relation to our simulations. By comparing the values of σ for 12 galaxies, the authors found to be σ_2 to be smaller than σ_1 but they also precise that both definitions do not induce a significant difference in their measurements of the intrinsic scatter in $\log(M_\bullet)$.

Stellar mass

Secondly, we use from this study the bulge stellar mass for 34 early-type galaxies. The authors obtained the data in two different ways : 13 bulge stellar mass are taken from Häring & Rix (2004) (who used spherical Jeans models to fit stellar kinematics). The remaining masses are computed by multiplying the V-band luminosity with the bulge mass-to-light ratio (M/L) derived from kinematics and dynamical modeling of stars or gas. The authors add that because some galaxies exhibit contradictions between the dynamical estimates of M/L and estimates of M/L from stellar population synthesis models, they chose to assign a minimum error of 0.24 dex to each value of stellar mass. While the bulge stellar mass is different by definition than the total stellar mass, it is considered that for galaxies with $M_* > 10^{11} M_\odot$, galaxies are bulge-dominated, i.e. the Bulge-to-Total (B/T) stellar mass ratio is approximately equal to 1. Therefore we will, similarly to several studies, approximate $M_* \approx M_{bulge}$.

Black hole mass

finally, the black hole mass sample from this paper is an update of a previous compilation of 67 dynamical black hole measurements from the authors, presented in McConnell et al. (2011b). The full sample is a survey of the literature originally made by Gültekin et al. (2009b), as they made a list of dynamically detected central BHs, starting with the compilations of Tremaine et al. (2002), Marconi & Hunt (2003), Ferrarese & Ford (2005),

and Graham (2008) and they only included direct dynamical measurements.

3.2. Datasets from Kormendy & Ho (2013)

$M_\bullet$ and σ

The authors of this paper used black hole mass and velocity dispersion for 45 elliptical galaxies taken from various sources in the literature (Nowak et al. (2008), Rusli et al. (2013), Gültekin et al. (2009a), Gültekin et al. (2009b), Walsh et al. (2010), Schulze & Gebhardt (2011) and others.)

They define σ as the intensity-weighted mean of $V^2 + \sigma^2$ out to a fixed fraction of the effective radius r_e that contains half of the light of the galaxy. The authors also explain that when calculating σ from photometry and published kinematics, they adopt the fraction $r_e/2$. We use their sample to represent their galaxies on a $M_\bullet - \sigma$ relation plot and also show the best fit that they found.

$M_\bullet$ and M_*

Similarly, the authors constructed a sample of bulge stellar masses taken from various sources in the literature. Instead of using the individual measurement of bulge stellar mass for each galaxy, we will simply take the best linear fit they obtained : $\log_{10}\left(M_\bullet/10^8 M_\odot\right) = (1.49^{+0.06}_{-0.05}) + (1.16 \pm 0.08)\cdot \log_{10}\left(M_{\rm bulge}/10^{11} M_\odot\right)$.

Dark matter mass

We also use from this study the power law relations they obtained for the $M_\bullet - M_{DM}$ scaling relation. There are two power laws as the authors divide the galaxies into two dark matter halo mass bins : $M_{DM} < 10^{12} M_\odot$ and $M_{DM} > 10^{12} M_\odot$.

They obtained $M_\bullet \propto M_{DM}^{2.7}$ and $M_\bullet \propto M_{DM}^{0.34}$ respectively. The authors used a $M_* - M_{DM}$ relation found by Behroozi et al. (2010), arguing that many papers found similar results. They then used the estimation we mentionned above that $M_* \approx M_{bulge}$ and the $M_\bullet - M_{bulge}$ relation we use : $M_\bullet \propto M_{bulge}^{1.16}$. This allows them to obtain the two $M_\bullet - M_{DM}$ relations we will be using.

3.3. Datasets from Sabra et al. (2015)

From this study we extract their fit for the $M_\bullet - \sigma$ computed from their sample of galaxies. To build this sample that have dynamical $M_\bullet$ and v_c measurement they collected a large sample of 376 galaxies of all types for which measurements of $M_\bullet$, v_c, and/or σ exist. They compiled this sample from papers that present measurements of SMBH masses (among them McConnell & Ma (2013), Gültekin et al. (2009b), Pastorini et al. (2007), Ferrarese & Ford (2005), Peterson et al. (2004), Gebhardt et al. (2000)). and papers studying the $M_\bullet - \sigma$ relation (Hu (2009), Gültekin et al. (2009b) and others).

Starting with a total of 376 galaxies, only 125 of them have a $M_\bullet$ measurement. Filtering by taking galaxies with also a v_c or σ measurement resulted in 53 galaxies with both $M_\bullet$ and v_c and 89 galaxies with $M_\bullet$ and σ.

3.4. Other datasets considered

Finally, we will use three $M_\bullet - M_{DM}$ relations found in the literature :

- Di Matteo et al. (2003) : The authors used ΛCDM cosmological hydrodynamic simulations in order to obtain a $\sigma - v_c$ relation. They then used the measured $M_\bullet - \sigma$ relation from Tremaine et al. (2002) in order to link $M_\bullet$ and v_c. Finally, using the relation between the dark matter halo mass and the circular velocity of the galaxy, they obtained : $\left(\frac{M_\bullet}{10^8 M_\odot}\right) \sim 0.7 \left(\frac{M_{DM}}{10^{12} M_\odot}\right)^{4/3}$.
- Ferrarese (2002) : In this study, the author uses a previously measured $M_\bullet - \sigma$ relation as well as a $\sigma - v_c$ relation obtained using measurements from 38 galaxies. Then, using the simulated $M_{DM} - v_c$ relation from Bullock et al. (2001) finally gives : $\left(\frac{M_\bullet}{10^8 M_\odot}\right) \sim 0.10 \left(\frac{M_{DM}}{10^{12} M_\odot}\right)^{1.65}$.
- Baes et al. (2003) : This study also uses the simulated $M_{DM} - v_c$ relation from Bullock et al. (2001) and the observed $M_\bullet - \sigma$ relation from Tremaine et al. (2002). Combining them with the $\sigma - v_c$ they observe, they are able to find : $\left(\frac{M_\bullet}{10^8 M_\odot}\right) \sim 0.11 \left(\frac{M_{DM}}{10^{12} M_\odot}\right)^{1.27}$.

These three $M_\bullet - M_{DM}$ relations are therefore semi-observational relation as they use both results obtained with simulations and observations.

4. Numerical and fitting methods

In this study and generally in the literature, the scaling relations between the black hole mass and a property of the host's galaxy, are fitted in straight lines in log-log space:

$$\log_{10}(M_\bullet/10^8 M_\odot) = \alpha + \beta \cdot \log_{10} X \tag{3}$$

with $M_\bullet$ being the black hole mass in solar mass $M_\odot$ and X can be different quantities such as $X = \sigma/200{\rm kms}^{-1}$, $X = M_{\rm bulge}/10^{11} M_\odot$ or $X = M_{\rm DM}/10^{12} M_\odot$

Velocity dispersion

To compute the stellar velocity dispersion from the TNG simulation, we took in particular the central velocity dispersion, i.e. the velocity dispersion in a certain radius of aperture. First of all, we computed σ by taking it as the statistical dispersion of velocities about the mean velocity of stars in the radius considered. To be consistent with the literature and common used methods, we chose as statistical dispersion the standard deviation, defined as :

$$\sigma = \sqrt{\frac{1}{N}\sum_{i=1}^{N}(x_i - \mu)^2} \tag{4}$$

which is the relation for a sample of N values and μ is the mean value. The authors in McConnell & Ma (2013) measured the velocity dispersion for stars within a radius r with $r_{inf} < r < r_{eff}$ and $r_{inf} = GM_\bullet\sigma^{-2}$ and r_{eff} is the effective radius or half-light radius which is the radius at which half of the total light of a galaxy is emitted.

Thus, for reasons of simplicity, we considered the assumption that the light of stars is directly related to their mass and thus the radius or half-light radius is equal to the half-mass radius. This is particularly useful for us because the TNG project allows to determine the half-mass radius of a galaxy but not its half-light

radius. Therefore we computed the central velocity dispersion as σ in the half-mass radius.

Stellar mass

For the stellar mass, as explained previously, McConnell & Ma (2013) takes into consideration the bulge stellar mass. However, the TNG project does not allow to easily compute the bulge stellar mass as there is no feature that determines the limitation of the bulge. It would have been possible to consider the bulge as a sphere of arbitruary size centered around the galaxy's SMBH, for example of size 3kpc. This assumption could also be an important factor of error as the bulge radius depends on multiple factors such as the size, type, age or shape of the galaxy and would have been incredibly time-consuming numerically wise. This is why we didn't consider any radius of stellar mass and simply took the entire stellar mass of the galaxies.

As mentionned previously, we consider that the total stellar mass is approximately equal to the bulge stellar mass. This assumption is motivated by the fact that massive galaxies are more bulge-dominated and the majority of the observed galaxies from McConnell & Ma (2013) have a bulge tellar mass $M_* > 10^{11} M_\odot$, meaning that they are relatively massive galaxies.

Dark matter mass

Finally, we extract from the TNG simulations the dark matter halo mass which is an existing feature allowed by the TNG project. We study the $M_\bullet - M_{DM}$ relation for galaxies with M_{DM} ranging from $10^{11} M_\odot$ to $10^{14} M_\odot$. The TNG project allows us to directly obtain the dark matter halo mass of a galaxy while most astronomical observations determine the dark matter mass using the circular veloxity or velocity dispersion with semi-observational models (i.e. models that combine observations and simulations).

5. SMBH - Host galaxy scaling relations

First, we will try to see if the relations considered hold, i.e. if the TNG simulations are in agreement with the observational dataset taken in the literature, at redshift $z = 0$. These comparisons will help us confirm the numerical model as well as the robustness of the observations, determine the limits of the simulations (in resolution or in method) or the limits of observation and will enable us to look at the evolution of the relation for different redshift. We will also study the relations for different simulations (TNG50, TNG100 and TNG300) as well as for different type of galaxies in the simulations (central halo galaxies or central and satellites halo galaxies).

5.1. Relations at redshift $z = 0$

5.1.1. SMBH mass - velocity dispersion : $M_\bullet - \sigma$

We first study the $M_\bullet - \sigma$ relation at redshift $z = 0$ presented on Fig. 1. We computed the $M_\bullet - \sigma$ using TG100. For comparison, we have plotted the best fitting $M_\bullet$-σ relations from the observations by McConnell & Ma (2013), Kormendy & Ho (2013) and Sabra et al. (2015) (solid orange, blue and pink line respectively) for the panel at redshift $z = 0$. We also plotted on the Figure the data points observed in McConnell & Ma (2013), Kormendy & Ho (2013) (grey errorbars).

Looking at the figure, there seems to exist a $M_\bullet - \sigma$ correlation when simulated with TNG100. and the observational datasets we use to compare to the simulation also show a correlation.

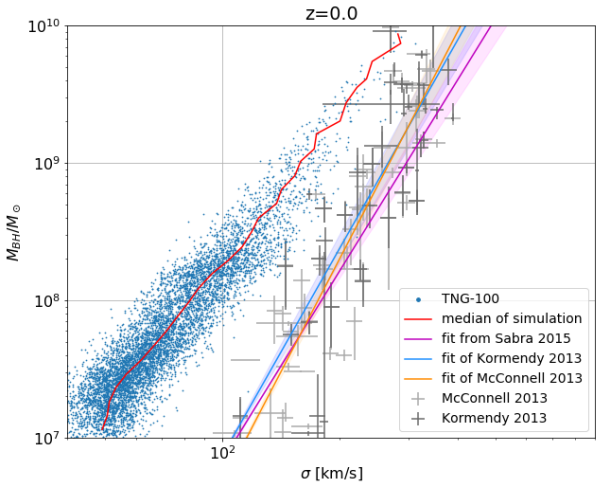

Fig. 1. SMBH mass - host galaxy velocity dispersion relation in TNG100. The panel is showing the $M_\bullet - \sigma$ relation at redshift 0 compared with the observed datasets and best-fits from McConnell & Ma (2013), Kormendy & Ho (2013) and Sabra et al. (2015). which are also measured at redshift 0. The colored zones around the fit lines represent the uncertainty on the best fit and not on the measurements.

However, the discrepancy is striking : the simulated $M_\bullet - \sigma$ relation is off-setted in comparison to the different observed $M_\bullet - \sigma$ correlations. The off-set could be considered in two different ways : our simulation produces galaxies with a velocity dispersion being too low (the relation is thus shifted to the left on the $M_\bullet - \sigma$ diagram), or the simulated SMBHs are overly-massive (therefore creating an upward shift on the diagram). However, the black hole mass function in TNG is in relative good agreement with observations (Sijacki et al. (2015)) and TNG100 also produces a quasar luminosity function at low redshift that agrees well with the observations (Weinberger et al. (2018), Habouzit et al. (2019)), suggesting that TNG100 doest not produce in general overly massive black holes for $M_\bullet > 10^7$ in the near Universe. Therefore the discrepancy in the $M_\bullet - \sigma$ relation should be mainly due to the computation, simulation or observation of σ.

Another remarkable difference on Fig. 1 is between the slope of the simulated $M_\bullet - \sigma$ relation and the observed ones. Keeping in mind that the $M_\bullet - \sigma$ relation is fitted using : $\log_{10}(M_\bullet/10^8 M_\odot) = \alpha + \beta \cdot \log_{10}(\sigma/200\text{km/s})$, the slope in the log-log space is the value of β. The observed datasets produce values that can be found in Table 7.2.

In particular, McConnell & Ma (2013), Kormendy & Ho (2013), Sabra et al. (2015), Ferrarese (2002) found respectively $\beta = (5.73 \pm 0.32)$; (5.02 ± 0.38); (4.60 ± 0.31) and (4.50 ± 0.52).

The $M_\bullet - \sigma$ relation presented on Fig. 1 corresponds to TNG100 for central galaxies in Table 7.2 and we obtained $\beta = (3.67 \pm 0.04)$. The difference is important and we will see later in Section 5.3.1 that other considerations of type of galaxies and other TNG simulations also don't attain good agreement with the observations.

Although our simulations tend to produce $M_\bullet - \sigma$ relation with smaller slopes than in observations, there have been numerous observational datasets that have produce a broad range of values for the slope. The first published estimates of β varied from ~ 3.75 Gebhardt et al. (2000) up to values of ~ 4.8 for Ferrarese & Merritt (2000) and Merritt & Ferrarese (2001). As we see with more recent studies such as Kormendy & Ho (2013) and McConnell & Ma (2013), the range of slope values

seems to be increasing as they both obtained values over 5, even approaching 6 for the later.

To tackle this problem, there have been studies and hypothesis conducted to explain this range. First, the authors from Merritt & Ferrarese (2001) argued in their study that the measurements of σ are polluted partly by the use of a regression algorithm that ignores measurement errors and partly by the incorrect choice for the dispersion of the Milky Way Galaxy. According to them, these effects create datasets producing low slopes ($\beta < 4$). However, Tremaine et al. (2002) support the argument that the explanations given in Merritt & Ferrarese (2001) account for at most a small part of the slope range. Their explanation is that the range of slopes arises mostly because of systematic differences in the velocity dispersions used by different groups for the same galaxies.

All these arguments allow us to understand how this broad range of slopes highlightes the difficulty to conduct these measurements and to use them with confidence. Our simulations also may need improvements as one possible argument to explain the discrepancy between the observed and our simulated slopes is that our definition to compute σ doesn't take into account phenomenons that impact the measure of σ. We recall that we computed σ as the standard deviation of the stars' velocity within the half-mass radius. For comparison, Li et al. (2020) computed σ_x which is the rest-frame SDSS-r band luminosity-weighted stellar line-of-sight velocity dispersion measured within a projected radius of 1.5 arcsec from galaxy center in x-projection. They add in the paper that by using the stellar-mass-weighted σ instead of the light-weighted σ, the $M_\bullet - \sigma$ relation steepens very slightly, but the general results are consistent, giving another possible way to compute σ in future studies. Their numerical definition of σ could be more accurate to compare it to observations as in McConnell & Ma (2013) they measured σ as a spatially resolved measurement of the line-of-sight velocity dispersion $\sigma(r)$ and radial velocity $v(r)$, integrated out to one effective radius. Indeed, our definition doesn't take into account dust in the line of sight which can largely impact the luminosity of stars during observations.

Now to tackle the problems posed by observations of σ, it may be possible to convert σ from measurements of v_c using existing $\sigma - v_c$ correlations as suggested in Di Matteo et al. (2003). Because measurements of σ are noisy and measurements of v_c, which are in fact measures of mass, are much less noisy, one possibility would be to take the best fit of the linear $\sigma - v_c$ relation as a tool for conversion. As the authors of the study explain, using σ introduces a significant source of artificial scatter in the $M_\bullet - \sigma$ relation. This hypothesis is however to consider with caution as our interest lies in the slope of the relation and the it is possible that the noise broadening the relation would have a minor impact on the slope.

5.1.2. SMBH mass - stellar mass : $M_\bullet - M_*$

We now shift our focus on the $M_\bullet - M_*$ scaling relation at redshift $z = 0$ presented on Fig. 2. We compare the relation obtained with the TNG-100 simulation to the observational data from McConnell & Ma (2013) which is also at redshift $z = 0$. As previously explained in Section 3, we compare on one hand the total stellar mass in TNG-100 to on the other hand the bulge stellar mass from the study. However the bulge stellar mass dominates the total stellar mass for massive galaxies and thus our comparison holds.

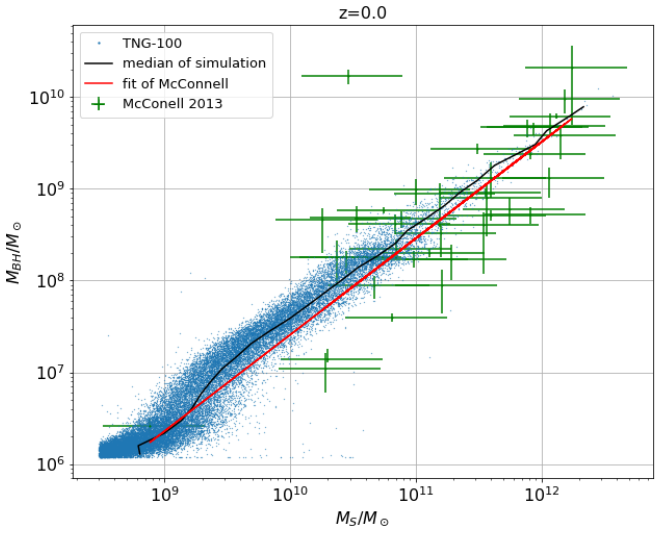

Fig. 2. $M_\bullet - M_*$ plane of the TNG100 simulation at $z = 0$ for BHs of MBH > 10^6 $M_\odot$ located in galaxies of M_* > 10^9 $M_\odot$. We show the $M_\bullet$-M_* relation for all galaxies in the simulation compared with the observed dataset (green points with errorbars) and best-fit (solid red line) from McConnell & Ma (2013) which is also measured for galaxies at redshift $z = 0$. We also show the $M_\bullet$-M_* median relations derived from the simulations at $z = 0$ (solid black line)

Again, the correlation between the SMBH mass and the total stellar mass of a galaxy is clear in TNG100. Moreover, this time the simulated $M_\bullet - M_*$ relation is in good agreement with the observation. Smilarly to the $M_\bullet - \sigma$, the relation is fitted using : $\log_{10}\left(M_\bullet/10^8 M_\odot\right) = \alpha + \beta \cdot \log_{10}\left(M_{bulge}/10^{11} M_\odot\right)$, and β is the slope of the relation. From the observational dataset we obtain $\beta = (1.05 \pm 0.13)$ while the simulated $M_\bullet - M_*$ slope on Fig. 2 gives a slope $\beta = (1.04 \pm 0.01)$ (see Table 7.2). However, our simulated $M_\bullet - M_*$ relation presents less scater in the range of $M_\bullet$. For a given stellar mass, observations tend to show a wider ranger of $M_\bullet$, an observation made by various studies working on the TNG simulations (Li et al. (2020), Weinberger et al. (2018), Terrazas et al. (2020)). The authors of Li et al. (2020) have demonstrated this tighter scatter in TNG100 while both Weinberger et al. (2018), Terrazas et al. (2020) focused on TNG300.

In our case, at $M_* \sim 10^{10.3} M_\odot$ the observational samples provides $M_\bullet$ ranging from $10^7 M_\odot$ to around $10^{8.6} M_\odot$ whereas our simulation produces a mean value of $10^{7.8} M_\odot$ with a scatter around $\sim 10^{0.3}$. Similarly, the BHs of $M_\bullet = 10^7 M_\odot$ are almost uniquely in galaxies with $M_* < 10^{10} M_\odot$. This phenomenon is observable for all stellar masses between $10^{10} M_\odot$ and $10^{10.2} M_\odot$. We thus have a tighter $M_\bullet - M_*$ relation, and for a fixed stellar mass, it produces a smaller diversity of black hole masses than in the sample from McConnell & Ma (2013), especially galaxies with lower BH mass. Looking at the right upper part of the Fig. 2 (i.e. for high $M_\bullet$ and high M_*), we observe that TNG100 is almost unable to produce galaxies in this region with the depletion starting at $M_* > 10^{11} M_\odot$, observations also made by Li et al. (2020).

Nonetheless, we should demonstrate some carefulness when comparing the simulated relation to the observed one because both can be biased for multiple reasons.

First of all, for the observed dataset, as pointed out in Habouzit et al. (2021), it is probable that we observe AGNs which are relatively not obscured, thus having a luminosity not affected. As Bernardi et al. (2007) explain in their study, a selection bias can happen for dynamically-measured BH sample. According to them, black hole abundances are often estimated using a measured correlation between black hole mass and another more easily measured property, for instance the velocity dispersion or bulge luminosity. The correlation between the black hole and this property is thus used to transform the distribution of the observable property into an estimate of the distribution of black hole masses. However this process can turn out to be problematic as different observables provide different estimates : using σ as observable will predict fewer massive black holes than using the luminosity (cf their study for further explanations on the matter). Also, we saw how the observed $M_\bullet - \sigma$ relation doesn't agree with our simulations, thus making us question the validity of this method since it is not clear if the measurements of σ suffer from a sort of bias or error.

Second of all, our simulations also suffer from choices we made and effects of bias. Indeed, for the stellar mass, as we mentionned in this report, we considered the total stellar mass of the galaxies in TNG and not the bulge stellar mass. To take rigorously into account only the bulge stellar mass we would have need to take every single galaxies one by one to inspect their shape or size for instance. Another thing that could have been done, as they do in Li et al. (2020), is to take the stellar mass within twice the stellar half mass radius. Following our explanations in Section 4, we note that another source of error can come from the fact that galaxies are seeded with a black hole of a precise mass when they reach a precise dark matter halo mass, creating a strong liaison between the two. Since the dark matter halo mass is correlated to the stellar mass (Girelli et al. (2020), Shuntov et al. (2022)), it is a source of bias in the $M_\bullet - M_*$ relation. On top of that, according to the authors of Hirschmann et al. (2010), the Central-limit theorem predicts that random merging of galaxies results in a decreasing scatter of the correlations between black hole mass and host bulge mass. Finally, Habouzit et al. (2021) also points out that the TNG simulations don't take into account that the value of the radiative efficiency is set partly by the spin of the black hole and the geometry of the accretion flow.

All these reasons lead us to hypothesize that without these numerical biases we would possibly obtain a broader $M_\bullet - M_*$ scatter, i.e. a larger range of $M_\bullet$ for a given stellar mass. It is also possible to consider that by removing the observational bias effects, it would result in a tighter scatter in the observational $M_\bullet - M_*$ relation. Thus, future observations and simulations face the challenge of taking into account all the selection effects and biases (observational and numerical) in order to comprehensively compare them.

5.1.3. SMBH mass - dark matter halo mass : $M_\bullet - M_{DM}$

Finally we look at the final scaling relation : $M_\bullet - M_{DM}$ that we present on Fig. 3. The Figure shows the $M_\bullet - M_{DM}$ relation obtained with TNG100 (grey points). We compare our results to Kormendy & Ho (2013), who divided the galaxies into two dark matter halo mass bins : $M_{DM} < 10^{12} M_\odot$ and $M_{DM} > 10^{12} M_\odot$.

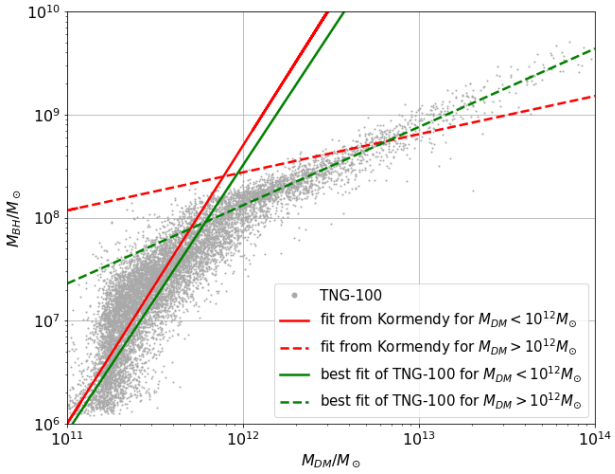

Fig. 3. SMBH - host galaxy dark matter halo mass relation in TNG100. The panel is showing the simulated $M_\bullet - M_{DM}$ relation at redshift 0 (grey points) . We compare the best-fits from our simulations to the best-fits from observational dataset in Kormendy & Ho (2013) which is also measured at redshift $z \sim 0$.

For each bin, we plot the best fit of our simulation and the best fit they obtained. We focus on the slope α of the fits and compare them in Table 7.3 to the observational values.

Looking at Fig. 3, we clearly see a break (or knee) in our simulated points in grey at $M_{DM} \sim 10^{12} M_\odot$ which justify the separations of galaxies into two bins. However there also seems to be a break for $M_{DM} \sim 3 \cdot 10^{11} M_\odot$. Having not found any study focusing on the $M_\bullet - M_{DM}$ for galaxies with a dark matter halo mass bigger or smaller than this value, we consider all galaxies with $M_{DM} < 10^{12} M_\odot$ together. The fit for the low mass bin obtained by Kormendy & Ho (2013) (solid red line) is very similar to ours (solid green line) with a slope $\alpha = 2.7$ and 2.59 respectively. However a discrepancy appears for the galaxies in the high mass bin : the observations found $\alpha = 0.34$ whereas we found $\alpha = 0.76$. On the Fig.3, the difference in the two fit is striking (dashed red line and dashed green line).

As suggested in Kormendy & Ho (2013), because the relation between $M_\bullet$ and M_{DM} is complicated and presents a break, it suggests that the growth of black holes is controlled by stellar mass and not DM mass.

5.2. Time evolution of scaling relations

We only study the time (i.e. redshift) evolution of the $M_\bullet - M_*$ relation as it is the only one of the three that is in good agreement with observations at redshift $z = 0$. We consider that there are numerical and/or observational challenges to solve for both $M_\bullet - \sigma$ and $M_\bullet - M_{DM}$ relations before examining their redshift evolution.

5.2.1. SMBH mass - stellar mass : $M_\bullet - M_*$

We present on Fig. 4 and Fig. 5 the time evolution of the $M_\bullet - M_*$ relation for $\sim$ 20 galaxies in TNG100. We also add on the $M_\bullet - M_*$ diagrams the best linear fit at redshift $z = 0$ from McConnell & Ma (2013). On the Fig. 5, we have two colorbars in order to study the time evolution either with the snapshot number or the redshift. Indeed TNG is divided into 100 snapshots taken during

the full time simulation with a corresponding redshift for each of them. One has to be careful for two reasons : a high redshift value corresponds to a small value for the snapshot number, and the snapshot number scale is linear while the redshift number is not (it rapidly decreases as the snapshot number increases then increases much more slowly as the snapshot number increases). In order to study how different galaxies evolve throught out the simulation, we investigate the time evolution of three different samples of $\sim$ 20 galaxies. Our samples of galaxies depend on their initial stellar mass, which we divided into three bins :

- Low starting mass : M_* between $10^8 M_\odot$ and $3 \cdot 10^8 M_\odot$ at $z \sim 7$. Their $M_\bullet - M_*$ time evolution is presented the left panel of Fig. 4.
- Intermediate starting mass : M_* between $10^9 M_\odot$ and $3 \cdot 10^9 M_\odot$ at $z \sim 7$ Their $M_\bullet - M_*$ time evolution is presented on the Fig. 5.
- High starting mass : M_* higher than $10^{10} M_\odot$ at $z \sim 7$ Their $M_\bullet - M_*$ time evolution is presented on the right panel of Fig. 4.

By initial conditions we mean galaxies at redshift $z \sim 7$ or snapshot number 11, as older (higher redshift) galaxies are rarely seeded with a black hole, thus making impossible the $M_\bullet - M_*$ study. Therefore, the goal is to study in the first time how galaxies evolve on the $M_\bullet - M_*$ diagram but also how their initial stellar mass influences their redshift evolution. The first observation we can make on Fig. 5 and 4 is how low redhisft galaxies are generally in good agreement with the linear fit from observations. This reinforces our previous conclusion that TNG is able to retrieve a similar $M_\bullet - M_*$ relation to observations at low redshift. Secondly, a striking observation is that in TNG, there seems to be different phases of BH growth for the low and intermediate starting BH masses (Fig. 5 and 4) :

- First phase of BH growth: during the first phase, BHs practically don't even grow while the stellar mass rapidly increases, thus shifting the colored points to the right. Habouzit et al. (2021) made a similar observations and argue that a strong feedback from SNe in TNG100 is responsible for delaying the first episode of gas accretion.
- Later phases of BH growth: Once the BHs start growing, they grow very efficiently, creating a very steep slope on the diagram for M_* between $10^{10} M_\odot$ and $4 \cdot 10^{10} M_\odot$. When the galaxies reach a stellar mass around $4 \cdot 10^{10} M_\odot$, their position on the diagram is close to the observational linear fit. From there, galaxies generally evolve linearly along the linear fit until they reach their final position.

Finally, looking at the final position of galaxies on the $M_\bullet - M_*$ for Fig. 5 and Fig. 4, we remark that galaxies starting with a similar stellar mass can end up with broadly different stellar mass. Indeed, some galaxies finish their evolution on the $M_\bullet - M_*$ diagram at $M_* \sim 10^{11} M_\odot$ while others are able to reach $M_* > 10^{12} M_\odot$. Because this observation holds for all bins of stellar mass, we conclude that the starting stellar mass does not really impact the final stellar mass of a galaxy. The same observations can be made with the BH mass.

For the time evolution of galaxies with high starting stellar mass ($> 10^{10} M_\odot$) on Fig. 4, some observations can be made :

- First phase of BH growth: as opposed to the other two bins of mass, the BH mass and stellar mass grow rapidly, thus shifting the colored points towards the linear fit of observations. The $M_\bullet - M_*$ relation presents a very large scatter compared to the previous time evolutions.
- Later phases of BH growth: Once the BHs have grown and the galaxies' position on the $M_\bullet - M_*$ diagram are on the linear fit, the galaxies generally evolve linearly along the linear fit until they reach their final position.
- Again, the galaxies have a broad range of final stellar mass with some ending at $M_* \sim 10^{11} M_\odot$ while others are able to reach stellar masses well over $M_* > 10^{12} M_\odot$.

We conclude that regardless of the starting bin of stellar mass, there doesn't seem to be a clear correlation between the final stellar mass of a galaxy and its stellar mass during the early time of the simulation.

We also show on Fig. 6 the simulated $M_\bullet - M_*$ relation for redhsifts going from 0 to 4. We see how at redshift 0 the simulation gives a linear relation with a very small knee at $M_* \sim 2 \cdot 10^9 M_\odot$. We see how this knee grows and is more pronounced when the redshift of the simulation increases. This knee can be observed on the Fig. 5 and the left panel of Fig. 4 which separates the two different phases of BH growth.

5.3. Relations for different type of galaxies and different TNG simulations

Finally, we shift our focus on how the three scaling relations change when considering all or only central galaxies and when considering other simulations than TNG100. Previously, we explored the relations using TNG100 and central galaxies for the $M_\bullet - \sigma$ and $M_\bullet - M_{DM}$ relations and all galaxies for the $M_\bullet - M_*$ relation. The mass of BHs in massive galaxies is often determined by dynamical measurements, which is only possible for close systems. In observations, these rare massive galaxies are often found on the center of clusters. It is therefore necessary to study the relations using only central galaxies. However, we also seek to determine how the relations change when we considered the other type of galaxies. On top of that, comparing different simulations could help us understand some discrepancies we obtained with observations.

5.3.1. SMBH mass - velocity dispersion : $M_\bullet - \sigma$

We summarize in Table 7.2 in Appendix 7.2 the different results we obtained when simulating the $M_\bullet - \sigma$ relation. As previously, we study the relation by computing it in logarithmic space as : $\log_{10}\left(M_\bullet / 10^8 M_\odot\right) = \alpha + \beta \cdot \log_{10}\left(\sigma / 200\right)$ and we focus on the β values. We also add in the Table 7.2 the observational values found in the literature. As discussed before, the observational values for the $M_\bullet - \sigma$ relation slope range from (4.50 ± 0.52) for Ferrarese (2002) to (5.73 ± 0.32) for McConnell & Ma (2013) and the simulation we studied is TNG100 for central galaxies giving a slope $\beta = (3.67 \pm 0.04)$.

Looking at the simulated values in the Table, there seems to be two phenomenons happening :

- When considering central galaxies the slope tends to be steeper than with all galaxies. For TNG100, the slope increases from (3.35 ± 0.08) to (3.67 ± 0.04), for TNG300 it

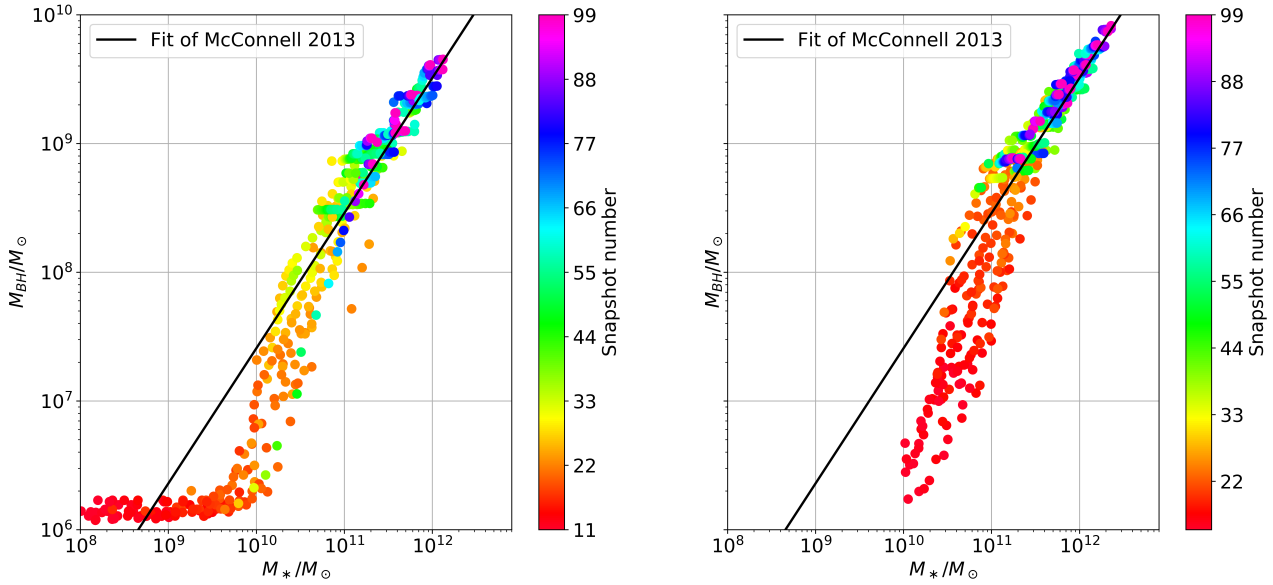

Fig. 4. $M_\bullet - M_*$ diagram for a sample of $\sim$ 20 galaxies with an initial stellar mass ranging from $10^8 M_\odot$ to $3 \cdot 10^8 M_\odot$ (left panel) and mass bigger than $10^{10} M_\odot$ (right panel). The black solid line represents the $M_\bullet - M_*$ best linear fit at redshift $z = 0$ from McConnell & Ma (2013).

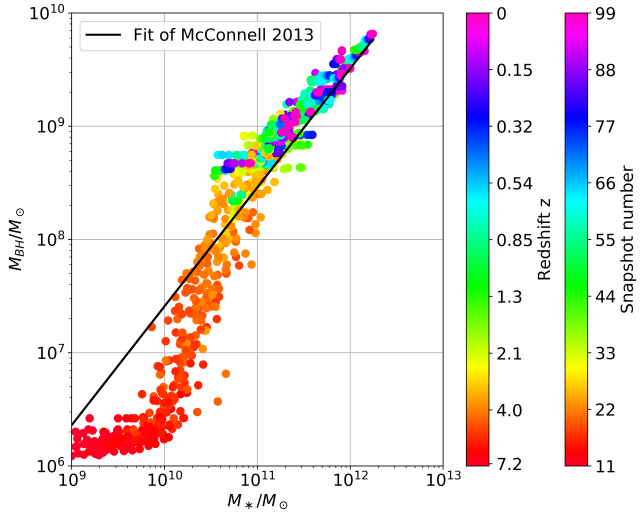

Fig. 5. $M_\bullet - M_*$ diagram for a sample of $\sim$ 20 galaxies with an initial stellar mass between $10^9 M_\odot$ and $3 \cdot 10^9 M_\odot$. The black solid line represents the $M_\bullet - M_*$ best linear fit at redshift $z = 0$ from McConnell & Ma (2013).

increases from (3.80 ± 0.06) to (3.97 ± 0.07) and for TNG50 in increases from (3.21 ± 0.07) to (3.65 ± 0.06).

- The TNG300 simulation gives a steeper slope than TNG100, whether we take all galaxies or central galaxies. We show on Fig. 7 the results for TNG100 and TNG300 with central galaxies. It is not clear to us why TNG100 provides a smaller slope value.
- The TNG50 gives results with the biggest discrepancy with the observations.

Simulations using central galaxies look to be giving bigger values of slope, that is to say values closer to observational values. This is maybe because, as mentionned, in observations massive galaxies are usually located in the center of clusters. Using central galaxies may thus seem as the best possibility to conduct our simulations. Regarding which size of simulation use between 100 and 300, both shown on Fig. 7, there are discrepancies. On top of giving a steeper slope, TNG300 gives a much broader relation than TNG100. It also seems that for low BH mass, the relations can't be confidently fitted using a linear fit, which is true for TNG100 and especially for TNG300. As the BH mass increases, the relation tightens and can be more easily fitted by a linear relation.

As explained previously, we can't assert with enough certainty which slope is the correct one as observations and simulations give a broad range of values as both are polluted by selection biases or numerical uncertainties. It is not clear if our simulations underestimate the value of the slopes or if observations overestimate them or if both happend. It is however unlikely that the correct estimation of β is at one end of the spectrum of values, being 3.35 and 5.73 considering the uncertainty of other values. These relatively important uncertainty values ($\sim$ 10%) overlap for some observations and simulations. It is therefore necessary to conduct measurements and simulations of higher precision in order to rule out with certitude the possibility that the slope values don't agree. Recent studies have sparked a discussion on the exact slope of the relation and it is argued that these differences can be ascribed to different fitting techniques, different samples and different measures of the velocity dispersion.

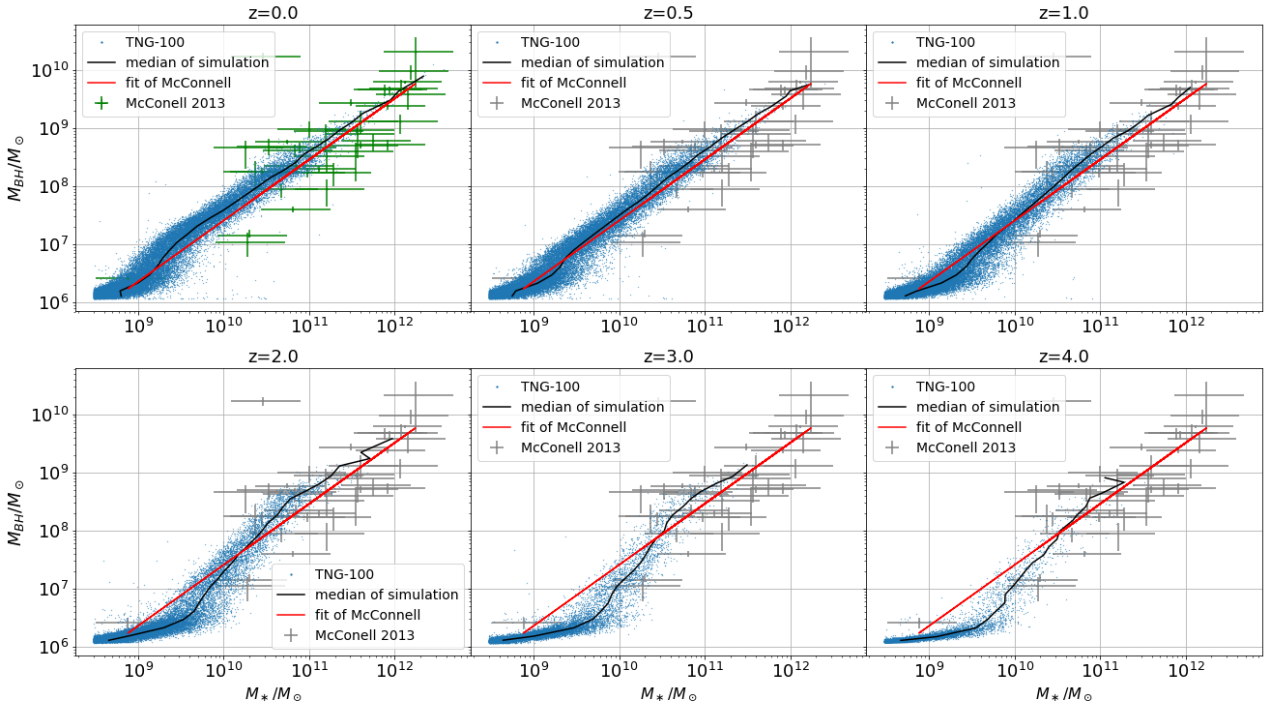

Fig. 6. $M_\bullet - M_*$ diagram at different redshifts using TNG100. In each panel we plot the observed datasets from McConnell & Ma (2013) but higlight it in green only for the $z = 0$ panel as the measurements are made at redshift 0. On each panel we also plot the median of the TNG simulation as well as the best fit of the observations.

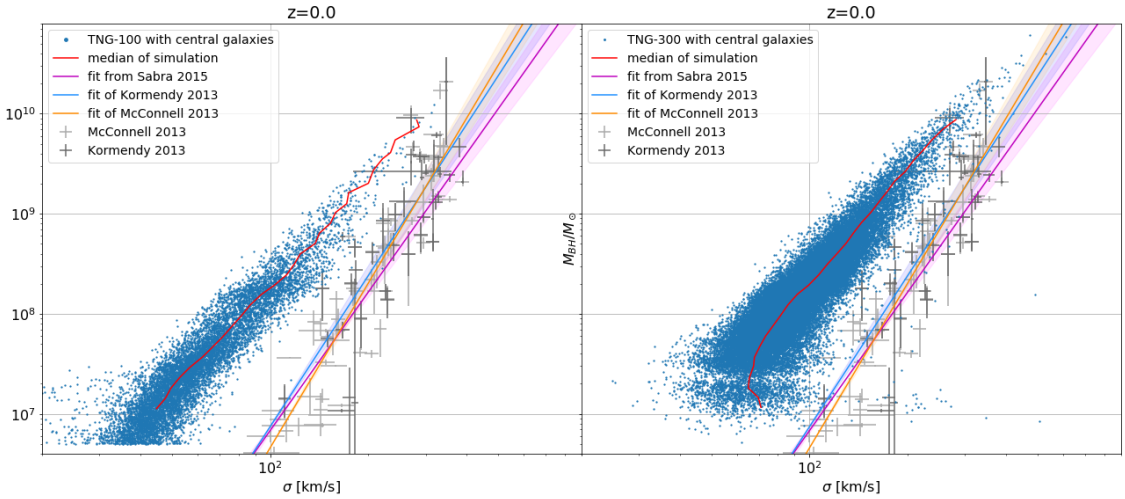

Fig. 7. SMBH mass - host galaxy velocity dispersion correlations in TNG100 and TNG300. The panels are showing the $M_\bullet - \sigma$ relation for central galaxies using TNG100 (left panel) or TNG300 (right panel) compared with the observed dataset and best-fit from McConnell & Ma (2013), Kormendy & Ho (2013) and Sabra et al. (2015). The observed data are measured for galaxies at redshift 0 and the simulations are also done at redshift $z = 0$

5.3.2. SMBH mass - stellar mass : $M_\bullet - M_*$

We summarize in Table 7.2 in Appendix 7.2 the different results we obtained when simulating the $M_\bullet - M_*$ relation. As previously, we study the relation by computing it in logarithmic space as : $\log_{10}\left(M_\bullet/10^8 M_\odot\right) = \alpha + \beta \cdot \log_{10}\left(M_{\rm bulge}/10^{11} M_\odot\right)$ and focus on the β values. We also add in the Table 7.2 the observational values found in the literature. As discussed before, the observational values for the $M_\bullet - M_*$ relation slope are in good agreement with the values obtained with simulations, expect for TNG300 with central galaxies. McConnell & Ma (2013) reported in their study a slope $\beta = (1.05 \pm 0.13)$ while we found similar values

: (1.04 ± 0.01), (1.06 ± 0.04) and (1.02 ± 0.01) for TNG100 and TNG300 with all galaxies and TNG100 with central galaxies respectively. We can make additional remarks on the simulations :

- As opposed to with $M_\bullet - \sigma$, the results of TNG100 are very similar for both types of galaxies considered ((1.04 ± 0.01) and (1.02 ± 0.01) for all galaxies and central galaxies respectively) as seen on Fig. 8. Similarly, this observation can be made for the TNG50 simulations where the slope values are equal (0.92 ± 0.01) for all galaxies or only central galaxies.

- It is unclear to us why such discrepancy happens between the different simulations with TNG300 ((1.06 ± 0.04) and (1.25 ± 0.01) for all galaxies and central galaxies respectively). The discrepancy between both simulations is clearly visible on Fig. 9. We see on the right panel how TNG300 with central galaxies produces a relation with a clear different slope than in observations and on top of that the simulation is off-setted.

- The left panel of Fig. 9 shows the $M_\bullet - M_*$ relation using TNG300 with all galaxies. Whilst the slope is good agreement with the observations, there seems to be a slight off-set between the median of the simulation and the linear best-fit of observations.

- TNG50 gives smaller values than the other simulations and observations.

As opposed to the $M_\bullet - \sigma$ relation, using central galaxies doesn't give better results than when using all galaxies and, for TNG300, it is even the opposite. Also, this time TNG100 seems to be producing results closer to observations than the other siimulations. Nonetheless, we consider that it is possible that the correct estimation of β is close to the observational value as it is corroborated by differents simulations we conducted.

5.3.3. SMBH mass - dark matter halo mass : $M_\bullet - M_{DM}$

Finally, we summerize in Table 7.3 the different results we obtained for the $M_\bullet - M_{DM}$ relation. This time we only investigate how the relation changes for different TNG simulations and we always take central galaxies. We study the relation by focusing on the power law between the BH mass and dark matter halo mass $M_\bullet \propto M_{DM}^{\alpha}$, thus looking for α. We first study the relation when separating the galaxies in two dark matter bins ($M_{DM} < 10^{12} M_\odot$ and $M_{DM} > 10^{12} M_\odot$) and compare it to the the observed relation from Kormendy & Ho (2013). Then we study how the relation changes when we consider the entire spectrum of dark matter mass ($10^{11} M_\odot < M_{DM} < 10^{14} M_\odot$) and compare it to the results of Di Matteo et al. (2003), Ferrarese (2002) and Baes et al. (2003). We make the following remarks regarding the analysis using two mass bins :

- We recall that Kormendy & Ho (2013) found for α 2.7 and 0.34 for $M_{DM} < 10^{12} M_\odot$ and $M_{DM} > 10^{12} M_\odot$ respectively. We also recall that TNG100 procuded a value in good agreement (2.59) for the smaller mass bin but with a discrepancy (0.76) for the higher mass bin.

- TNG100, 300, 50 produce very different values for the low mass bin (2.59, 6.44, 1.60 respectively) but relatively similar values for the high mass bin (0.76, 0.81 and 0.65 respectively).

- TNG100 produces the relation in best agreement with observations when considering both bins. Although TNG50 has the closest value for the high mass bin to the observed one, because the value of α for the low mass bin is much smaller than in observations, we consider TNG100 to produce the best results.

- The value of α for the low mass bin in TNG300 is more than two times bigger than in observations and in other simulations. This discrepancy is even more surprising considering how TNG300 produces a similar result to TNG100 and 50 for the high mass bin.

For the analysis using a single mass bin, we compare our results to Di Matteo et al. (2003), Ferrarese (2002) and Baes et al. (2003) who obtain $\alpha = 1.33, 1.65$ and 1.27 respectively. This time, all three TNG simulations produce a value for α in relatively good agreement with the results found in the literature (1.08, 1.22, 1.16 for TNG100, 300 and 50 respectively). It is interesting to see how when considering the low mass bin, TNG300 produces a relation that doesn't agree with either observations and simulations, while when considering all galaxies it produces a very similar result to other simulations and observations.

6. Conclusions

Throughout this report, we have studied the correlations between the mass of SMBHs and some properties of their host galaxies in different simulations of the IllustrisTNG project, mainly the TNG100 simulation. We studied in particular 3 scaling relations : the $M_\bullet - M_*$ relation, the $M_\bullet - \sigma$ and the $M_\bullet - M_{DM}$ relation. We have exmained the relations at redshift $z = 0$ and compared them to observational measurements made at redshift $z = 0$ found in the literature. These observational datasets handpicked from the literature were chosen without applying any selection biases. On top of that we have also studied how the $M_\bullet - M_*$ relation evolves in the TNG simulations as a function of the redshift and finally we tried to better understand how the three scaling relations change for different type of galaxies and for different simulations in the IllustrisTNG project. The main findings are summarized as follows :

- In the TNG100 simulations at redshift $z = 0$, $M_\bullet$ is correlated to σ, M_* and M_{DM} similarly to the observations taken in the literature. However, all relations in TNG are not able to produce the same agreement with observations. Indeed, the $M_\bullet - M_*$ relation presents the best agreement but still lacks some scatter in the range of $M_\bullet$. For a given stellar mass, observations tend to show a wider ranger of $M_\bullet$. Thus, for a fixed stellar mass, it produces a smaller diversity of black hole masses than in the sample from McConnell & Ma (2013).

- On the other hand, despite showing a clear correlation, the $M_\bullet - \sigma$ and $M_\bullet - M_{DM}$ relations show clear discrepancies with the observed correlations. Regarding the $M_\bullet - \sigma$ relation, the TNG simulations produce an off-set correlation, in other words the simulated relation is shifted to lower velocity dispersion values compared to observations. The discrepancy lies also in the difference of slope of the relations, with the observed correlations presenting a steeper

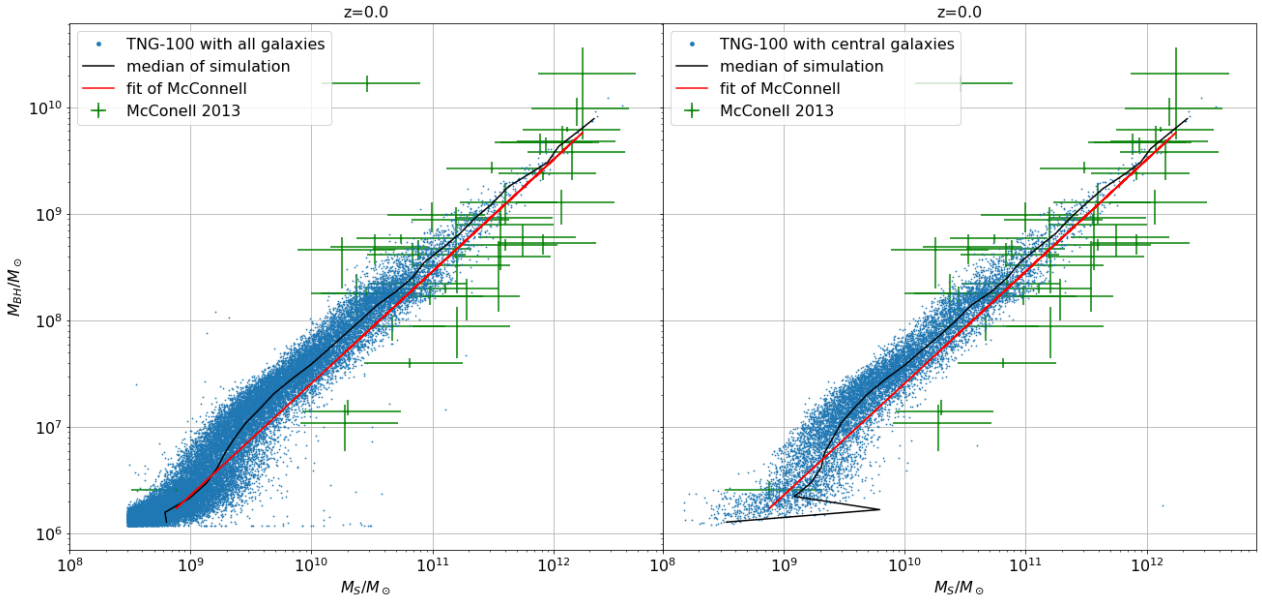

Fig. 8. SMBH-M$_*$ plane of the TNG100 simulation at $z = 0$ for BHs of MBH > 10^6 M$_\odot$ located in galaxies of M$_*$ > 10^9 M$_\odot$. We show the $M_\bullet$-M_* relation for all galaxies in the simulation (left panel) or only galaxies in the center of a halo (right panel) compared with the observed dataset (green points with errorbars) and best-fit (solid red line) from McConnell & Ma (2013) which is also measured for galaxies at redshift $z = 0$. In both figures, we show the $M_\bullet$-M_* median relations derived from the simulations at $z = 0$ (solid black line)

slope than ours. The observed slopes range between 4.5 and 5.7 while our values lie between 3.3 and around 4, up to uncertainty errors.

- The $M_\bullet - M_{DM}$ correlation is different from the first two because it can be splitted into two separate correlations. For galaxies with $M_* < 10^{12} M_\odot$, the TNG100 relation presents a slope in good agreement with the observed slope from Kormendy & Ho (2013) (2.59 and 2.7 respectively) but for galaxies with $M_* > 10^{12} M_\odot$, the discrepancy in the slope is clear (0.76 and 0.34). If we consider all galaxies as one part, ranging from $10^{11} M_\odot$ to $10^{14} M_\odot$, then TNG100 gives us a slope of 1.08 while Di Matteo et al. (2003), Ferrarese (2002) and Baes et al. (2003) obtained respectively a slope of 1.33, 1.65 and 1.27 using cosmological simulations, combined with theoretical prescriptions.

- The study of the time evolution of the $M_\bullet - M_*$ relation showed that for galaxies with a stellar mass $\sim 10^8$ or $10^9 M_\odot$ at redshift $z \sim 7$, the SMBHs practically don't grow while the stellar mass rapidly increases during first phase of evolution. The later phases see the SMBHs grow very efficiently and the galaxies follow the observed linear relation. We also investigated how the starting stellar mass is not correlated to the final (i.e. at $z = 0$) stellar mass as all starting stellar mass bins produce a broad range of final stellar mass. The galaxies with an initial stellar mass $\sim 10^{10} M_\odot$ present a larger scatter for the $M_\bullet - M_*$ relation until they reach the observational linear fit, that they then follow well.

- When studying the results with different TNG simulations and different choice of galaxies, TNG100 looks to be giving the results in best agreement with observations for the $M_\bullet - M_*$ relation. Using central or all galaxies does not produce significant differences, which can also be said for TNG50 but not for TNG300. For the $M_\bullet - \sigma$ relation, even though we can't attain results in good agreement with observations, using central galaxies gives results closest to observations. On top of that TNG300 seems to be giving the best results out of all simulations. Finally for the $M_\bullet - M_{DM}$ relation, TNG100 gives the results in best agreement with observations when considering to mass bins, although the high mass bin relation has a slight discrepancy. When considering all galaxies together, all three simulations produce similar results in agreement with observations.
- Therefore, between TNG100 and TNG300 there is no definitive simulation that gives the best results as it depends on the relation studied. However choosing central galaxies seems to be the best option to produce similar results to observations. As for TNG50, it produces underestimated values compared to the other silmulations for the $M_\bullet - M_*$ and $M_\bullet - \sigma$ relations.

It is important to note that the formation history (i.e. the evolution with the redshift) of a galaxy can greatly influences the properties that we observe (or simulate) at redshift $z = 0$. The three different relations in this report therefore need a particular focus on their redshift evolution to better understand how the complex interplay of physical processes impacts whether black holes co-evolve with some galaxies or properties. In this report, we have only submitted the $M_\bullet - M_*$ to the redshift evolution as it is the only one that presented strong enough consistency with the observational sample at redshift $z = 0$. Thus, it is also crucial to understand why the $M_\bullet - \sigma$ and $M_\bullet - M_{DM}$ relations present important discrepancies with the observations. The aim is to determine whether the simulations use models that don't faithfully reproduce some physical processes or whether there are measurement biases in the observations that induce uncertainty and errors which the simulations don't suffer from. Nonetheless, it is necessary to always confront our simulations to

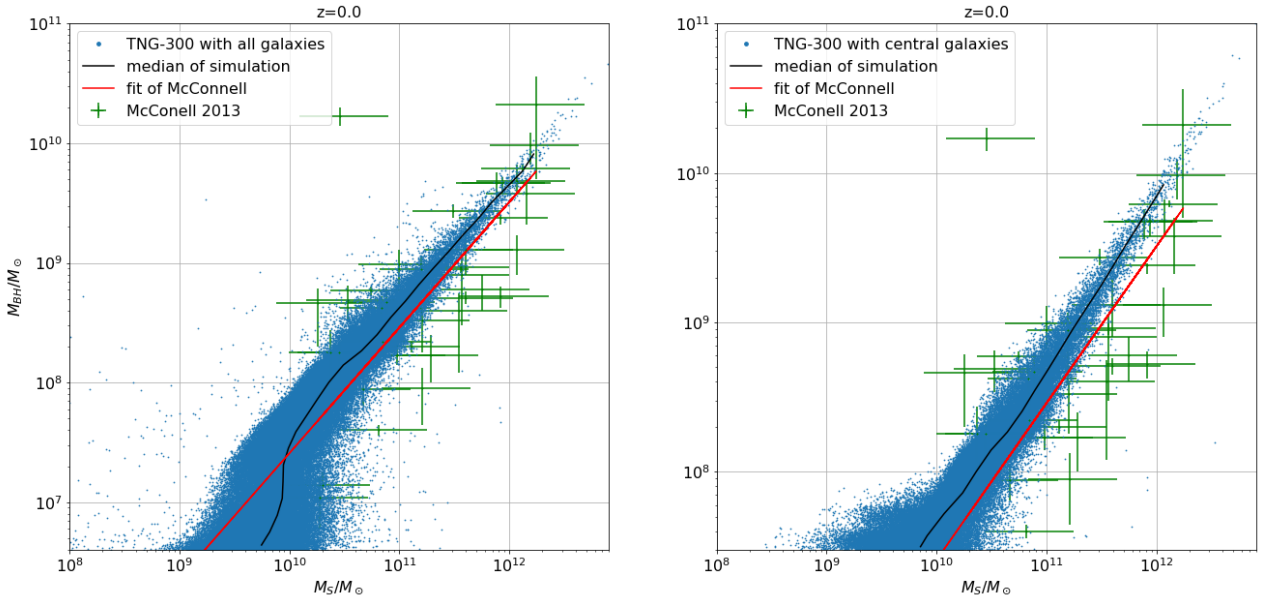

Fig. 9. SMBH-M$_*$ plane of the TNG300 simulation at $z = 0$ for BHs of MBH > 10^6 M$_\odot$ located in galaxies of M$_*$ > 10^9 M$_\odot$. We show the $M_\bullet$-M_* relation for all galaxies in the simulation (left panel) or only galaxies in the center of a halo (right panel) compared with the observed dataset (green points with errorbars) and best-fit (solid red line) from McConnell & Ma (2013) which is also measured for galaxies at redshift $z = 0$. In both figures, we show the $M_\bullet$-M_* median relations derived from the simulations at $z = 0$ (solid black line)

observations, as these observed datasets are powerful discriminants between models and the different implementations they use.

However, several things could have been done to improve most of the results we obtained. In the interest of time and efficiency we didn't explore these options but we will se now what could have improved our simulations.

First of all, for the stellar mass, as we mentionned in this report, we considered the total stellar mass of the galaxies in TNG and not the bulge stellar mass. To take rigorously into account only the bulge stellar mass we would have need to take every single galaxies one by one to inspect their shape or size for instance. Another thing that could have been done, as they do in Li et al. (2020), is to take the stellar mass within twice the stellar half mass radius. Regardless, as we discussed, the simulations are able to produce $M_\bullet - M_*$ scaling relations in general agreement with observations at z = 0, without however presenting a scatter as important as the observations.

Regarding the velocity dispersion and the $M_\bullet - \sigma$ relation, some very important improvements con be made. We computed σ as the standard deviation of the stars' velocity within the half-mass radius while Li et al. (2020) computed σ as the rest-frame SDSS-r band luminosity-weighted stellar line-of-sight velocity dispersion. Their definition of σ could be more accurate to compare it to observations as in McConnell & Ma (2013) they measured σ as a spatially resolved measurement of the line-of-sight velocity dispersion.

Finally, the possibility that the $M_\bullet - \sigma$ relation cannot be well described with a linear fit has to be considered. Indeed, Li et al. (2020) argued that the $M_\bullet - \sigma$ relation in TNG100 cannot be well described with a linear fit, with the relation having a break at $\log_{10}(\sigma) \sim 2.1$, but with our definition of σ we couldn't make such clear observation for TNG100. However, as mentionned, TNG100 and 300 with central galaxies can't be well described and fitted using a linear relation for the low BH masses.

Finally, to study the $M_\bullet - M_{DM}$ relation, we could have computed the dark matter halo mass differently. Indeed, studies in the literature generally construct semi-observational $M_\bullet - M_{DM}$ relation like in Di Matteo et al. (2003) where they start with a simulated $\sigma - v_c$ relation and then use both $M_\bullet - \sigma$ and $M_{DM} - v_c$ relations. Thus it would have been interesting to study how the $M_\bullet - M_{DM}$ changes when we compute M_{DM} by using our values of σ and injecting them into $\sigma - M_{DM}$ relations found in the literature.

It would also have been interesting to use results that don't depend on simulations as it is considered that they can't recreate faithfully every relations observed. For that, it would be possible for instance to reproduce the methods in Di Matteo et al. (2003) but using an observed $\sigma - v_c$ relation.

On top of that, we suggest to use the observational dataset from Bandara et al. (2009), which is a measurement of the total mass of a sample of galaxies made with gravitational lensing. With the assumption that the total gravitational mass is equal to the mass of the dark matter halo we would just need now a measurement of $M_\bullet$ of these galaxies. Althought they don't provide proper measurements for the black hole mass of these galaxies, we could search the liteature for measurements of $M_\bullet$.

Acknowledgements.

7. Appendix

7.1. Appendix A : SMBH - Velocity dispersion

7.2. Appendix B : SMBH - Stellar mass

Theorically	$\log_{10}\left(M_\bullet/10^8 M_\odot\right) = \alpha + \beta \cdot \log_{10}\left(\sigma/200\right)$
Observations	Best fit of observations
McConnell & Ma (2013)	$\alpha = (0.33 \pm 0.05), \beta = (5.73 \pm 0.32)$
Kormendy & Ho (2013)	$\alpha = (0.38 \pm 0.10), \beta = (5.02 \pm 0.38)$
Merritt & Ferrarese (2001)	$\alpha = (1.30 \pm 0.36), \beta = (4.72 \pm 0.36)$
Sabra et al. (2015)	$\alpha = (0.22 \pm 0.06), \beta = (4.60 \pm 0.31)$
Ferrarese (2002)	$\alpha = (0.22 \pm 0.09), \beta = (4.50 \pm 0.52)$
Tremaine et al. (2002)	$\alpha = (0.13 \pm 0.06), \beta = (4.02 \pm 0.32)$
Simulations	Best fit of simulations
TNG100 for all galaxies	$\alpha = (1.21 \pm 0.20), \beta = (3.35 \pm 0.08)$
TNG300 for all galaxies	$\alpha = (1.41 \pm 0.19), \beta = (3.80 \pm 0.06)$
TNG50 for all galaxies only	$\alpha = (0.85 \pm 0.17), \beta = (3.21 \pm 0.07)$
TNG100 for central galaxies only	$\alpha = (1.34 \pm 0.10), \beta = (3.67 \pm 0.04)$
TNG300 for central galaxies only	$\alpha = (1.43 \pm 0.32), \beta = (3.97 \pm 0.07)$
TNG50 for central galaxies only	$\alpha = (1.36 \pm 0.03), \beta = (3.65 \pm 0.06)$

Table 1. SMBH mass - velocity dispersion fits in observations and simulations. We present five relations taken from observations and six relations obtained using simulations. The relation is written as the log-log space equation and we focus on the β coefficients.

Theorically	$\log_{10}\left(M_\bullet/10^8 M_\odot\right) = \alpha + \beta \cdot \log_{10}\left(M_{\rm bulge}/10^8 M_\odot\right)$
Observations	Best fit of observations
McConnell & Ma (2013)	$\alpha = (0.51 \pm 0.09), \beta = (1.05 \pm 0.13)$
Simulations	Best fit of simulations
TNG100 for all galaxies	$\alpha = (0.57 \pm 0.01), \beta = (1.04 \pm 0.01)$
TNG300 for all galaxies	$\alpha = (0.62 \pm 0.04), \beta = (1.06 \pm 0.04)$
TNG50 for all galaxies	$\alpha = (0.38 \pm 0.01), \beta = (0.92 \pm 0.01)$
TNG100 for central galaxies only	$\alpha = (0.57 \pm 0.01), \beta = (1.02 \pm 0.01)$
TNG300 for central galaxies only	$\alpha = (0.61 \pm 0.01), \beta = (1.25 \pm 0.01)$
TNG50 for central galaxies only	$\alpha = (0.37 \pm 0.01), \beta = (0.92 \pm 0.01)$

Table 2. SMBH mass - stellar mass fits in observations and simulations. We present a relation taken from observations and 6 relations obtained using simulations. The relation is written as the log-log space equation and we focus on the β coefficients.

Observations and simulations	Best fit for : $M_{DM} < 10^{12} M_\odot$	Best fit for : $M_{DM} > 10^{12} M_\odot$
Kormendy & Ho (2013)	$M_\bullet \propto M_{DM}^{2.7}$	$M_\bullet \propto M_{DM}^{0.34}$
TNG100	$M_\bullet \propto M_{DM}^{2.59}$	$M_\bullet \propto M_{DM}^{0.76}$
TNG300	$M_\bullet \propto M_{DM}^{6.44}$	$M_\bullet \propto M_{DM}^{0.81}$
TNG50	$M_\bullet \propto M_{DM}^{1.60}$	$M_\bullet \propto M_{DM}^{0.65}$

Semi-observations and simulations	Best fit for : $10^{11} M_\odot < M_{DM} < 10^{14} M_\odot$
Di Matteo et al. (2003)	$M_\bullet \propto M_{DM}^{1.33}$
Ferrarese (2002)	$M_\bullet \propto M_{DM}^{1.65}$
Baes et al. (2003)	$M_\bullet \propto M_{DM}^{1.27}$
TNG100	$M_\bullet \propto M_{DM}^{1.08}$
TNG300	$M_\bullet \propto M_{DM}^{1.22}$
TNG50	$M_\bullet \propto M_{DM}^{1.16}$

Table 3. SMBH mass - dark matter halo mass fits in observations, semi-observations and simulations. In the upper part of the Table is the relation when the galaxies are divided in two categories and in the lower part when they are considered together. We compare one observation and three simulations in the upper part and three semi-observations and three simulations in the lower part. The relations are written as a power law equation. Semi-observation refers to results taken from the literature that combine simulations and observations.

7.3. Appendix C : SMBH - Dark matter halo mass

References

Anglés-Alcázar D., Özel F., Davé R., 2013, ApJ, 770, 5
Arav N., Borguet B., Chamberlain C., Edmonds D., Danforth C., 2013, MNRAS, 436, 3286
Bañados E., et al., 2018, Nature, 553, 473
Baes M., Buyle P., Hau G. K. T., Dejonghe H., 2003, MNRAS, 341, L44
Bandara K., Crampton D., Simard L., 2009, ApJ, 704, 1135
Behroozi P. S., Conroy C., Wechsler R. H., 2010, ApJ, 717, 379
Beifiori A., Courteau S., Corsini E. M., Zhu Y., 2012, MNRAS, 419, 2497
Bernardi M., Sheth R. K., Tundo E., Hyde J. B., 2007, ApJ, 660, 267
Booth C. M., Schaye J., 2009, MNRAS, 398, 53
Bullock J. S., Kolatt T. S., Sigad Y., Somerville R. S., Kravtsov A. V., Klypin A. A., Primack J. R., Dekel A., 2001, MNRAS, 321, 559
Cano-Díaz M., Maiolino R., Marconi A., Netzer H., Shemmer O., Cresci G., 2012, A&A, 537, L8
Carniani S., et al., 2015, A&A, 580, A102
Cattaneo A., et al., 2009, Nature, 460, 213
Chartas G., Brandt W. N., Gallagher S. C., Garmire G. P., 2003, in AAS/High Energy Astrophysics Division #7. p. 53.02
Choi E., Ostriker J. P., Naab T., Johansson P. H., 2012, ApJ, 754, 125
Choi E., Somerville R. S., Ostriker J. P., Naab T., Hirschmann M., 2018, ApJ, 866, 91
Cicone C., et al., 2014, A&A, 562, A21
Ciotti L., Ostriker J. P., 2001, ApJ, 551, 131
Croton D. J., et al., 2006, MNRAS, 365, 11
Davé R., Anglés-Alcázar D., Narayanan D., Li Q., Rafieferantsoa M. H., Appleby S., 2019, MNRAS, 486, 2827
Debuhr J., Quataert E., Ma C.-P., 2011, MNRAS, 412, 1341
Di Matteo T., Croft R. A. C., Springel V., Hernquist L., 2003, ApJ, 593, 56
Fabian A. C., 2012, ARA&A, 50, 455
Faucher-Giguère C.-A., Quataert E., 2012, MNRAS, 425, 605
Ferrarese L., 2002, ApJ, 578, 90
Ferrarese L., Ford H., 2005, Space Sci. Rev., 116, 523
Ferrarese L., Merritt D., 2000, ApJ, 539, L9
Feruglio C., et al., 2015, A&A, 583, A99
Gadotti D. A., Kauffmann G., 2009, MNRAS, 399, 621
Gebhardt K., et al., 2000, ApJ, 539, L13
Girelli G., Pozzetti L., Bolzonella M., Giocoli C., Marulli F., Baldi M., 2020, A&A, 634, A135
Graham A. W., 2007, MNRAS, 379, 711
Graham A. W., 2008, ApJ, 680, 143
Graham A. W., Onken C. A., Athanassoula E., Combes F., 2011, MNRAS, 412, 2211
Greene J. E., et al., 2010, ApJ, 721, 26
Gültekin K., et al., 2009a, ApJ, 695, 1577
Gültekin K., et al., 2009b, ApJ, 698, 198
Habouzit M., et al., 2019, MNRAS, 484, 4413
Habouzit M., et al., 2021, MNRAS, 503, 1940
Häring N., Rix H.-W., 2004, ApJ, 604, L89
Hirschmann M., Khochfar S., Burkert A., Naab T., Genel S., Somerville R. S., 2010, MNRAS, 407, 1016
Hu J., 2008, MNRAS, 386, 2242
Hu J., 2009, arXiv e-prints, p. arXiv:0908.2028
Jardel J. R., et al., 2011, ApJ, 739, 21
Kauffmann G., Haehnelt M., 2000, MNRAS, 311, 576
Kormendy J., 1993, in Dejonghe H., Habing H. J., eds, Vol. 153, Galactic Bulges. p. 209
Kormendy J., Gebhardt K., 2001, in Wheeler J. C., Martel H., eds, American Institute of Physics Conference Series Vol. 586, 20th Texas Symposium on relativistic astrophysics. pp 363–381 (arXiv:astro-ph/0105230), doi:10.1063/1.1419581
Kormendy J., Ho L. C., 2013, ARA&A, 51, 511
Kormendy J., Richstone D., 1995, ARA&A, 33, 581
Kormendy J., Bender R., Cornell M. E., 2011, Nature, 469, 374
Koudmani S., Henden N. A., Sijacki D., 2021, MNRAS, 503, 3568
Leighly K. M., Terndrup D. M., Baron E., Lucy A. B., Dietrich M., Gallagher S. C., 2014, ApJ, 788, 123
Li Y., et al., 2020, ApJ, 895, 102
Marconi A., Hunt L. K., 2003, ApJ, 589, L21
Marinacci F., et al., 2018, MNRAS, 480, 5113
McAlpine S., et al., 2016, Astronomy and Computing, 15, 72
McAlpine S., Bower R. G., Harrison C. M., Crain R. A., Schaller M., Schaye J., Theuns T., 2017, MNRAS, 468, 3395
McConnell N. J., Ma C.-P., 2013, ApJ, 764, 184
McConnell N. J., Ma C., Graham J. R., Gebhardt K., Lauer T. R., Wright S. A., Richstone D. O., 2011a, in American Astronomical Society Meeting Abstracts #217. p. 422.06
McConnell N. J., Ma C.-P., Gebhardt K., Wright S. A., Murphy J. D., Lauer T. R., Graham J. R., Richstone D. O., 2011b, Nature, 480, 215
McConnell N. J., Ma C.-P., Murphy J. D., Gebhardt K., Lauer T. R., Graham J. R., Wright S. A., Richstone D. O., 2012, ApJ, 756, 179
McLure R. J., Dunlop J. S., 2002, MNRAS, 331, 795
McNamara B. R., Nulsen P. E. J., 2007, ARA&A, 45, 117
Merritt D., Ferrarese L., 2001, ApJ, 547, 140
Moe M., Arav N., Bautista M. A., Korista K. T., 2009, ApJ, 706, 525
Mortlock D. J., et al., 2011, Nature, 474, 616
Naiman J. P., et al., 2018, MNRAS, 477, 1206
Nelson D., et al., 2018, MNRAS, 475, 624
Nelson D., et al., 2019, MNRAS, 490, 3234
Nowak N., Saglia R. P., Thomas J., Bender R., Davies R. I., Gebhardt K., 2008, MNRAS, 391, 1629
Omma H., Binney J., Bryan G., Slyz A., 2004, MNRAS, 348, 1105
Pastorini G., et al., 2007, A&A, 469, 405
Peterson B. M., et al., 2004, ApJ, 613, 682
Pillepich A., et al., 2018, MNRAS, 475, 648
Pillepich A., et al., 2019, MNRAS, 490, 3196
Reines A. E., Volonteri M., 2015, ApJ, 813, 82
Rosas-Guevara Y., Bower R. G., Schaye J., McAlpine S., Dalla Vecchia C., Frenk C. S., Schaller M., Theuns T., 2016, MNRAS, 462, 190
Rusli S. P., et al., 2013, AJ, 146, 45
Sabra B. M., Saliba C., Abi Akl M., Chahine G., 2015, ApJ, 803, 5
Saglia R. P., et al., 2016, ApJ, 818, 47
Sani E., Marconi A., Hunt L. K., Risaliti G., 2011, MNRAS, 413, 1479
Schaye J., et al., 2015, MNRAS, 446, 521
Schulze A., Gebhardt K., 2011, ApJ, 729, 21
Shankar F., et al., 2019, MNRAS, 485, 1278
Shuntov M., et al., 2022, A&A, 664, A61
Sijacki D., Vogelsberger M., Genel S., Springel V., Torrey P., Snyder G. F., Nelson D., Hernquist L., 2015, MNRAS, 452, 575
Springel V., Di Matteo T., Hernquist L., 2005, MNRAS, 361, 776
Springel V., et al., 2018, MNRAS, 475, 676
Terrazas B. A., Bell E. F., Henriques B. M. B., White S. D. M., Cattaneo A., Woo J., 2016, ApJ, 830, L12
Terrazas B. A., et al., 2020, MNRAS, 493, 1888
Thomas N., Davé R., Anglés-Alcázar D., Jarvis M., 2019, MNRAS, 487, 5764
Tombesi F., 2015, in Ness J.-U., ed., The Extremes of Black Hole Accretion. p. 12
Tremaine S., et al., 2002, ApJ, 574, 740
Volonteri M., Dubois Y., Pichon C., Devriendt J., 2016, MNRAS, 460, 2979
Walsh J. L., Barth A. J., Sarzi M., 2010, ApJ, 721, 762
Walsh J. L., van den Bosch R. C. E., Barth A. J., Sarzi M., 2012, ApJ, 753, 79
Weinberger R., et al., 2018, MNRAS, 479, 4056
Wyithe J. S. B., 2006, MNRAS, 365, 1082
van den Bosch R. C. E., 2016, ApJ, 831, 134